Electron Devices Society

# Design, Fabrication, Modeling and Characterization of a Polyimide-Based Membrane for High Strain Studies in Microfabricated Devices

Loïc Lahaye, Nicolas Roisin, Nicolas André, Denis Flandre, *Senior Member, IEEE*, and Jean-Pierre Raskin, *Fellow, IEEE*

***Abstract*—This paper reports the design, integration, modeling and characterization of single crystalline (c-Si) resistors on a 3.6 $\mu$m-thick and 2.7 mm-diameter polyimide MEMS membrane. We propose a straightforward *top-down* fabrication scheme to integrate any microfabricated devices onto a flexible membrane. A *bulge-test* setup is assembled to measure the deflection of the membrane under a white light interferometer. In addition, a finite elements method (FEM) model is introduced to predict the behavior of the membrane under increasing pressure up to 80 kPa. The parameters of the FEM simulation are tuned with the deflection results to extract the strain tensor, showing a maximal biaxial strain of 0.37% at 80 kPa in the 300 nm-thick c-Si devices. Raman spectroscopy is finally employed to confirm the FEM results by comparing the estimated Raman peak-shift with actual Raman measurements. The shift predicted using phonon-deformation potential (PDP) theory shows excellent agreement with the experimental validation, giving confidence in the FEM model.**

***Index Terms*—Flexible MEMS, polyimide membrane, strain, comsol.**

## I. Introduction

STRAIN engineering of micro-fabricated devices is a very active and ever-growing scientific enquiry. Be it in the field of performance improvement of devices [1], [2], sensing [3] or in the world of material science [4].

A popular choice for strain induction, is to rely on the mismatch between two material's thermal expansion coefficient generating stress during the fabrication process [5], [6]. This approach lead to the development of MEMS-based techniques allowing strain studies to be carried out up to the mechanical limits of the material [7], [8]. However, those techniques do not provide a dynamical control of the induced strain. Different devices, tailored to reach various strains, must be fabricated to cover a large range of deformation with sufficient step resolution. This leads to process and design complications as well as device-to-device variation in the measurement.

Received 15 January 2025; revised 5 March 2025; accepted 31 March 2025. Date of publication 3 April 2025; date of current version 24 April 2025. This work was supported by the joint PDR / Suisse FRS-FNRS / SNF Project between the EPFL (École polytechnique fédérale de Lausanne) in Switzerland and the UCLouvain in Belgium. The review of this article was arranged by Editor Philip Feng. *(Corresponding author: Loïc Lahaye.)*

The authors are with the Institute of Information and Communication Technologies, Electronics and Applied Mathematics (ICTEAM), UCLouvain, 1348 Louvain-la-Neuve, Belgium (e-mail: loic.lahaye@uclouvain.be).

Digital Object Identifier 10.1109/TMAT.2025.3557763

Another approach is to actively induce strain in a material or device via an external actuation mechanism. One technique is to rely on a bulge or blister test using a micro-fabricated membrane subject to increasing pressure. One way to do so is to use a thin, stress compensated, oxide based, membrane carrying the device or material of interest. While this approach has been extensively studied, as reported in [9], [10], it is generally used for pressure sensing rather than for inducing high strain. Indeed, those membranes are prone to breaking and typically allow to reach strain of up to 0.04% as in [11]. Other fabrication processes, like Silicon-on-Nothing (SON), can be used to build the membrane but they face similar challenges while only reaching 0.036 % of strain [12].

A promising path to reach higher strain levels is to build the membrane out of a polymer. The lower Young's modulus of polymers allows for more bulging and deformation of the membrane before fracture, which enables to induce a higher strain in the device or material of interest. A first example comes from [13] which integrates a 2D-layer of $MoS_2$ onto PDMS and reaches between 2 and 3 % of strain during the blister test. Another one, from [14], reports the integration of 10 nm-thick silicon resistors on a polyimide (PI) membrane. They demonstrate the induction of 3.5 % of strain in the silicon resistors [14].

While the use of PDMS or polyimide allows to reach high strain in the studied material, the practice comes with some drawbacks. The first one is bound to the use of soft plastics that exhibit poor resistance to heat or strong chemicals [15]. This renders them incompatible with many conventional processing techniques. The integration of electronic devices or material must be done via either a direct low temperature deposition, like in [15], or complex transfer and subsequent alignment of electronic layers, like in [14]. Other examples of flexible electronic processing, that illustrate their complex nature, are otherwise well described in the literature, including [16], [17], [18], [19]. A further issue is the lack of fundamental understanding of the mechanics governing the behavior of these flexible media. While conventional MEMS membranes benefit from a rich literature allowing to predict both the behavior of the membrane and the strain induction in the device under test [20], [21], [22], [23], [24], this is not the case for complex polymeric stacks. Furthermore, the strain field in the active material layer is often

2993-1576 © 2025 IEEE. All rights reserved, including rights for text and data mining, and training of artificial intelligence and similar technologies.
Personal use is permitted, but republication/redistribution requires IEEE permission. See https://www.ieee.org/publications/rights/index.html for more information.

Authorized licensed use limited to: Univ Catholique de Louvain/UCL. Downloaded on October 28,2025 at 09:29:17 UTC from IEEE Xplore. Restrictions apply.

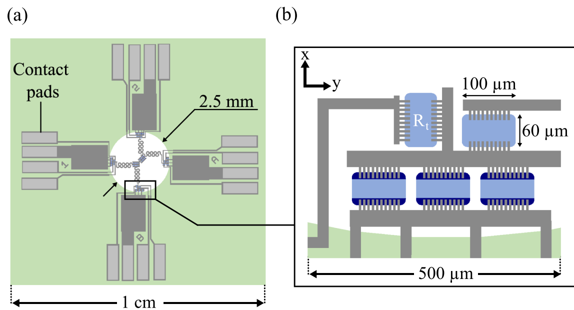


Fig. 1. Design schematics: (a) Layout showing a $1 \times 1$ cm$^2$ die featuring a 2.5 mm-diameter circular membrane. (b) Zoom on a subset of devices located on the membrane edge. $R_t$ stands for transversal resistor regarding the orientation of its electrical connections relative to $\varepsilon_{xx}$ in local coordinate. The $x$ and $y$ axis are shown as black arrows.The aluminium lines are in gray, the pad openings in light gray, the membrane in white and the die in light green. NPN devices and other resistors are visible on the layout but out of the scope of this work.

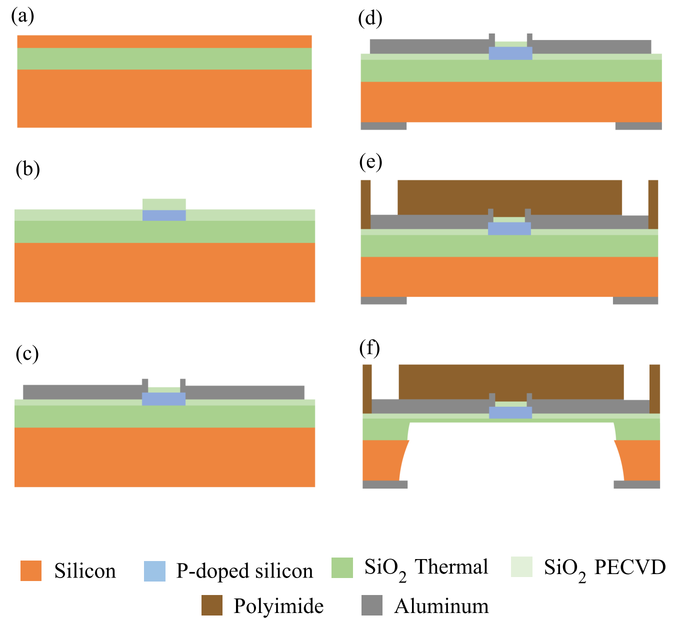


Fig. 2. Process flow schematics: Summary of the fabrication process used to integrate silicon resistors on a large, free standing, polyimide membrane. (a) Initial (100) SOI wafer with a top 300 nm c-Si layer, 1050 nm buried oxide (X) and c-Si substrate. (b) ICP-RIE patterning, doping and passivation with 180 nm of PECVD silicon dioxide of the top silicon to pattern 60 $\mu$m by 100 $\mu$m p-type c-Si mesas. (c) Electrical contacts deposition by sputtering a 600 nm-thick Al/Si layer, patterned with dry etching. (d) Back grinding of the c-Si substrate and definition of a 300 nm-thick aluminium mask. (e) Spin coating of a 3.6 $\mu$m-thick polyimide layer and contact pads opening by laser etching. (f) Release of the polyimide membrane by an isotropic $XeF_2$ dry etch of the c-Si substrate and isotropic BHF wet etch of the BOX.

simplified and treated as uniaxial or biaxial, like in [14], without formal validation which might prove detrimental in experiments requiring precise knowledge of the strain field components.

This work proposes both a simplified processing scheme for straightforward fabrication of flexible membrane for high-strain studies and a complete study of the mechanical behavior of the stack. The presented process integrates single crystal silicon (c-Si) devices with electrical connections on a 3.6 $\mu$m-thick and 2.7 mm-diameter PI membrane, without process limitation or complex layer transfer. In addition, a finite element method (FEM) model is built to study both the evolution of the membrane deflection and the strain field induced in the active silicon. In this study, the complete strain tensor is extracted from the FEM simulation, without assuming a particular shape of the strain field. To check the validity of our FEM model, a compact bulge test setup is introduced to pressurize the membrane and study its behavior both under a white-light interferometer and a Raman spectrometer.

## II. Fabrication

### A. Design

Fig. 1(a) represents the layout of a die carrying a 2.5 mm-diameter circular membrane. Each die features four sets of two c-Si p-type resistors and four NPN junctions positioned alongside the membrane's perimeter to maximise the amount of induced strain [10], [12]. All devices share the same 60 $\mu$m by 100 $\mu$m dimensions as visible in Fig. 1(b). Electrical connections are made by 1 $\mu$m-wide aluminium fingers and 20 $\mu$m-wide aluminium traces that extend from the die onto the released membrane. 500 $\mu$m by 1500 $\mu$m contact pads are visible in light gray on the figure. The study carried out in this work is performed on $R_t$ which stands for transversal resistor. It is defined by the current flowing perpendicularly to the direction of the $\varepsilon_{xx}$ strain component in local coordinate. All other structures visible on the layout are out of the scope of this paper.

### B. Process

The integration of p-type silicon resistors on a thin polyimide membrane is illustrated in Fig. 2. The process starts in Fig. 2(a) with a silicon-on-insulator (SOI) wafer from *SOITEC* featuring a top 300 nm-thick (100) oriented c-Si layer, a buried oxide (BOX) of 1050 nm and a bulk c-Si substrate of 725 $\mu$m.

To define the resistors, 60 $\mu$m by 100 $\mu$m silicon mesas are patterned in Fig. 2(b) by photolithography and anisotropic $CHF_3$ inductively coupled plasma reactive ion etching (ICP-RIE from *Corial*). The top silicon layer is thermally oxidized as a preparation step for ion implantation resulting in a 27 nm-thick silicon dioxide layer. A boron implantation step is performed to obtain p-type resistors. The implantation was performed by *Ion Beam Service (IBS)* with a requested dose of $4.2 \times 10^{13}$ atoms/cm$^2$ at an energy of 10keV. Doping atoms are then activated by a 30-minutes-long annealing at 850° C to complete the implantation phase. The final boron atom concentration in the silicon is estimated using a Silvaco Athena simulation to reach a maximal value of $3.5 \times 10^{18}$ cm$^{-3}$. A 180 nm-thick silicon dioxide layer is then deposited by plasma-enhanced chemical vapour deposition (PECVD by *Oxford Instruments*) to passivate the doped silicon resistors after stripping of the top 27 nm-thick thermal oxide used for the implantation process.

Fig. 2(c) deals with the electrical contacts definition. Access to the silicon mesas are first opened in the top silicon dioxide layer by a photolithographic step and a buffered HF ($HF + NH_4F$ in a 1:7 ratio) isotropic wet etch. The electrical connections are then built by sputtering (using a machine from *VST)* a 600 nm layer of Al/Si (99% aluminium and 1% silicon) next defined by photolithography and ICP-RIE $BCL_3$ anisotropic dry etch.

Authorized licensed use limited to: Univ Catholique de Louvain/UCL. Downloaded on October 28,2025 at 09:29:17 UTC from IEEE Xplore. Restrictions apply.

A 432° C thermal annealing under a flow of forming gas is finally performed to obtain an ohmic contact between the p-doped silicon and the aluminium.

Fig. 2(d) summarizes the preparation required for the release of the membrane. The wafer is first back-grinded from 725 $\mu$m to 280 $\mu$m in order to reduce the time needed to release the membrane. A 300 nm-thick aluminium mask is deposited by thermal evaporation (evaporator from *VST*) and patterned by photolithography and $H_3PO_4$ isotropic wet etch on the back side of the wafer to define the membrane geometries.

Polyimide is chosen as flexible substrate, as in [14], [25], and its integration as the last layer is done by spin coating a PI precursor as shown in Fig. 2(e). A commercial solution from *HDMicroSystem*, PI2545 [26], is used along with VM652, an adhesion promoter [27] from the same company. After priming of the wafer top surface with VM652, PI2545 is spun at a speed of 1500 rpm and cured at 350°C during one hour [26]. A final cured PI thickness of 3.6 $\mu$m is measured by ellipsometry. Access to the contact pads is then opened with a maskless picosecond-laser etching step (by *Oxford Instruments*). At this stage the wafer is diced to form 1 cm by 1 cm dies. As illustrated in Fig. 1(a), each die carries one 2.5 mm-diameter membrane.

Fig. 2(f) illustrates the membrane release which was done in two consecutive steps. A dry isotropic $XeF_2$ etch of the back c-Si is done (machine from *Xatic*), resulting in a slight 100 $\mu$m over etch and a final membrane of 2.7 mm-diameter.

Finally, the BOX is thinned by a timed isotropic BHF wet etch. A residual silicon dioxide layer of around 200 nm-thick is left to avoid the BHF to enter in direct contact with the silicon devices on the membrane's back side. Fig. 3(a) shows a picture of a released membrane.

We believe that the proposed method represents a potential simplification compared to [14] since it relies on a *top-down* integration scheme instead of a transfer of the active layer.

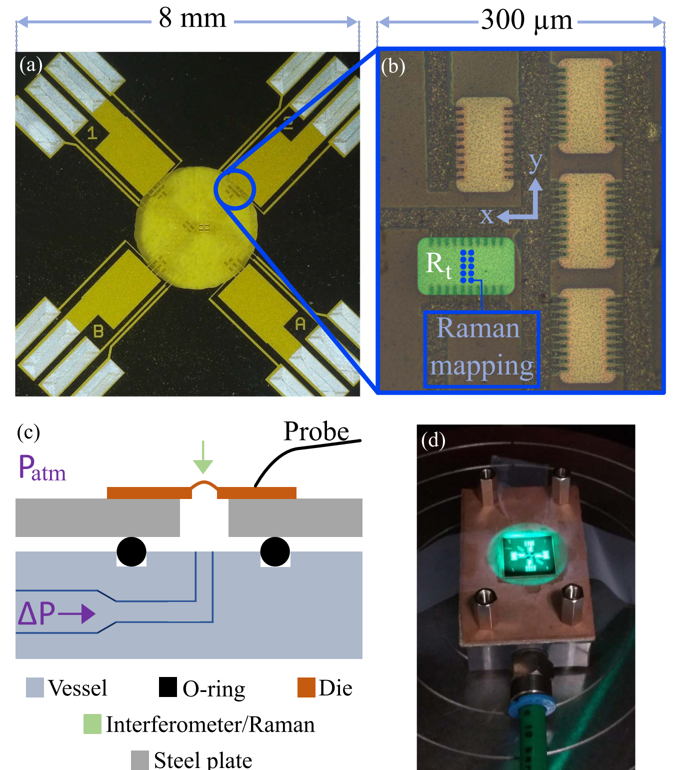


Fig. 3. Sample and instrumentation setup: (a) Top view of a 3.6 $\mu$m-thick and 2.5 mm-wide polyimide membrane. (b) Zoom on a subset of devices positioned along the membrane's edge. The device highlighted in green is a p-type resistor arranged in a transverse configuration regarding the direction of the current relative to the direction of the strain. The blue dots represent the 10 mapping points measured by the Raman spectroscope. Uncolored devices are out of the scope of this paper. (c) Pressurisation setup with a die featuring a membrane glued on a steel plate fixed to a pressure vessel. Air tightness is ensured by an O-ring. A pressure generator is connected at the inlet $\Delta P$. This setup can be set under a Michelson interferometer or a Raman spectroscope. The devices are electrically contacted by probes mounted on micromanipulators. (d) Picture of the experimental bulge test setup.

## III. Materials and Methods

### A. Simulation Framework

Due to the radical differences between the presented membrane stack which uses a low Young's modulus polyimide and a conventional silicon bulk micro-machined or stress compensated MEMS membrane, the behavior of our platform could not be predicted by usual analytic models like in [20], [22]. Furthermore, preliminary experimental tests, informed us that the stack enters in a plastic deformation regime passed a certain pressure level. This renders the use of analytical models for large deflection membranes like the ones of [28], [29], [30] impossible as well. A FEM simulation framework that takes into account plastic deformation has been developed using *Comsol Multiphysics* and is used to predict the deflection profile of the membrane and the evolution of the strain field in the c-Si resistors as a function of the applied pressure.

The model is built according to the real dimensions of the as-fabricated membrane to take into account the process non-idealities such as the over-etch. The simulation model is made out of a stack comprising a 200 nm-thick thermal silicon dioxide layer, the active 300 nm-thick patterned c-Si, the 180 nm-thick PECVD silicon dioxide layer and a 3.6 $\mu$m-thick polyimide layer similar to the one presented in Fig. 2. A 2.7 mm-diameter circular membrane with c-Si devices located around its perimeter is simulated. The materials Young's moduli are set to 87 GPa [31] and 2.7 GPa [26] for the $SiO_2$ and PI, respectively. The stiffness matrix of silicon, $\mathbf{C_{Si}}$, is used to take into account the material anisotropy [32], [33]. In our case, the principal strain components, $\varepsilon_{xx}$ and $\varepsilon_{yy}$, are along $\mathrm{Si}_{\langle 110\rangle}$.

To simulate the mechanical behavior, the *Solid Mechanics* module from Comsol is used to compute the stress, strain and displacement of each node in the mesh. All implemented equations are describe in the software technical documentation [34].

Regarding the plastic behavior of the stack, the following *Swift* model is implemented into *Comsol* to compute the actual stress and stain levels in the plastic regime [35]:

$$\sigma_{\text{eff}} = \sigma_{\text{y,eff}} \left(1 + \frac{\varepsilon}{\varepsilon_{0,\text{eff}}}\right)^{n_{\text{eff}}} \tag{1}$$

$\sigma$ and $\varepsilon$ are the actual stress and strain while $\sigma_{\text{y,eff}}$, $\varepsilon_{0,\text{eff}}$ and $n_{\text{eff}}$ are respectively the effective yield stress, reference strain and hardening coefficients to be fitted on experimental data.

Authorized licensed use limited to: Univ Catholique de Louvain/UCL. Downloaded on October 28,2025 at 09:29:17 UTC from IEEE Xplore. Restrictions apply.

### B. Bulge Test Setup

An instrumentation setup is designed to allow the pressurisation of the PI membrane and induce strain in the silicon devices. The setup, illustrated in Fig. 3(c) and (d), is made out of a pressure vessel with a device mounted on top. The die to be tested is first glued on a steel plate with M-bond 200 [36]. The steel plate is pierced to allow the pressure to be transferred to the membrane. The sub-assembly is then mounted on the pressure vessel by four screws while an O-ring ensures proper sealing between the plate and the vessel.

The pressure vessel in itself is made out of a machined acrylic block to allow the connection of a pressure generator at the inlet $\Delta P$. The pressure generator is a KAL-100 from *Halstrup Walcher*, allowing the production of controlled pressure in the 0 to 100 kPa range with a 0.05% accuracy [37]. In this study, the maximum applied pressure is of 80 kPa. The whole assembly is compact enough to be placed under a white light interferometer or a Raman spectrometer as shown in Fig. 3(d).

### C. Deflection Measurement

The measurement of the deflection is carried out by a white light interferometer from *Polytec* [38]. This non-destructive measurement allows to obtain the local deflection profile of our bulged membrane [39].

A die carrying a 2.7 mm-diameter membrane is mounted on the bulge test setup and the deflection profile of the membrane is measured. The additional pressure above atmospheric, $\Delta P$, ranges from 1 to 80 kPa by steps of 1 kPa up to 22 kPa, 2 kPa up to 40 kPa and 4 kPa up to 80 kPa. The pressure is then lowered following identical steps down to 1 kPa. The 0 kPa pressure point is not measured because the released membranes do not always have a flat profile due to residual stress in the stack inducing buckling. The 1 kPa deflection level is taken as reference.

Raw measured Polytec profiles are leveled to remove the die inclination and fitted by a second-order least-square method. The maximal deflection points are detected and plotted as a function of the pressure for each bulged profile.

Measuring the evolution of the membrane maximal deflection as a function of the pressure is done to calibrate the simulation parameters. The $\sigma_{\text{y,eff}}$, $\varepsilon_{0,\text{eff}}$ and $n_{\text{eff}}$ parameters from the *Swift* model [35] are to be fitted on the data point from the white light interferometer to tune the simulation.

### D. Strain Field Raman Validation

In order to properly validate the strain field results obtained from the simulator, a Raman spectroscopy experiment was designed using a LabRAM HR from *Horiba Scientific* equipped with a 514 nm laser. This non-destructive measuring technique allows to obtain Raman spectra which are specific to every material since they depend on their structural configuration [40]. At rest, the Raman spectrum of (100) silicon is made out of one longitudinal optical (LO) mode centered around 520.7 cm$^{-1}$ [41]. Upon straining of the c-Si devices, the modification of the crystal lattice will result in a measurable shift of the Raman peak position which will be used to validate our simulation model [42].

Similarly to the deflection setup, the peak shift is measured for pressures ranging from 0 to 80 kPa with steps as described in Section III-C. The measurement is made using a 514 nm laser that first penetrates through the 3.6 $\mu$m-thick PI layer. The PI layer does not interfere with the experiment since polyimide features a low absorbance coefficient for green light [43] and only features Raman peaks far from the one of c-Si, at above 1000 cm$^{-1}$ [44].

A 10-point mapping is done at each pressure step by measuring the Raman response of the silicon device at 10 different locations of $R_t$ as illustrated in Fig. 3(b). This mapping leads to noise and mismatch measurement reduction and allows the extraction of the average peak-shift value induced by strain in the silicon mesa.

Data processing starts by first averaging the 10 Raman spectra of each pressure point. The averaged peak is then normalized relative to its own maximum and the obtained data points are fitted by a Lorentzian function [40]. In the case of a (100) top plane c-Si, only the longitudinal optical mode is observable [45]. The maximum value hence corresponds to this LO peak which is detected around the initial 520.7 cm$^{-1}$ resting position. Doing this for each pressure step provides us with an experimental measurement of the peak shift as a function of the pressure.

No strong hypothesis can be made regarding the shape of the strain field induced in our c-Si devices. To validate our simulation results, we solve the eigen-value problem of [46] based on the secular matrix (2) shown at the botom of this page. It is used to compute the pressure-peak shift variation $\hbar\omega_i$ of the three Raman optical modes based on the full non-linear strain tensor given by the FEM simulation. Solving the eigenvalue's problem allows to find the three $\lambda_i$ and then the shifts using $\hbar\omega_i = \sqrt{\lambda_i - \omega_0^2}$ with $\hbar\omega_0 = 520.7$ cm$^{-1}$. Three parameters ($p$, $q$ and $r$) called the phonon deformation potential (PDP) coefficients are used. In this work, coefficients reported by [47] and [48] are used. Solving the eigenvalue problem based on (2) using the *Comsol* strain tensor will provide us with a theoretical estimation of the strain/peak-shift relation that will be compared with the actual Raman experimental data.

## IV. Results and Discussions

### A. Deflection Results

Deflection results of a 3.6 $\mu$m-thick and 2.7 mm-diameter polyimide membrane are presented in Fig. 4. A subset of five raw deflection profiles is illustrated in the figure's inset. A gradient of color from light to dark green is used to represent increasing

$$\begin{pmatrix} p\varepsilon_{11} + q\left(\varepsilon_{22} + \varepsilon_{33}\right) & 2r\varepsilon_{12} & 2r\varepsilon_{13} \\ 2r\varepsilon_{12} & p\varepsilon_{22} + q\left(\varepsilon_{33} + \varepsilon_{11}\right) & 2r\varepsilon_{23} \\ 2r\varepsilon_{13} & 2r\varepsilon_{23} & p\varepsilon_{33} + q\left(\varepsilon_{11} + \varepsilon_{22}\right) \end{pmatrix} \tag{2}$$

Authorized licensed use limited to: Univ Catholique de Louvain/UCL. Downloaded on October 28,2025 at 09:29:17 UTC from IEEE Xplore. Restrictions apply.

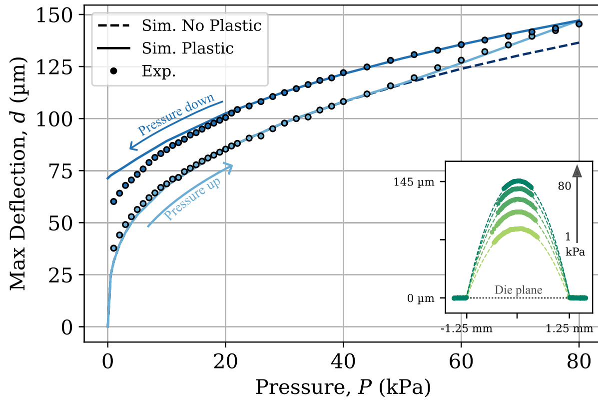


Fig. 4. Deflection measurement of a 3.6 $\mu$m-thick 2.7 mm-diameter circular polyimide membrane: The inset shows a selection of local deflection profiles under increasing pressure at 10, 20, 40, 60 and 80 kPa taken by a white light interferometer. The main plot shows the maximum of each raw deflection curve for pressure ranging between 1 and 80 kPa and then 80 to 1 kPa. Light and dark blue circles are used for experimental data point for the up and down pressure cycle, respectively. The plain lines represent the simulation considering plasticity for both the up and down pressure cycles with the same color code. The dashed line represents a simulation that does not consider plasticity.

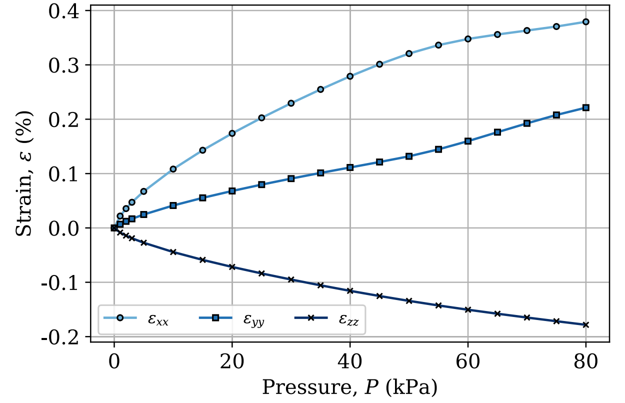


Fig. 5. Strain field simulation: Strain field inside a 0.3 $\mu$m-thick c-Si device on a 3.6 $\mu$m-thick 2.7 mm-diameter polyimide membrane under increasing pressure ranging from 0 to 80 kPa. Circles, squares and crosses are used to represent $\varepsilon_{xx}$, $\varepsilon_{yy}$ and $\varepsilon_{zz}$, respectively.

pressure levels at 10, 20, 40, 60 and 80 kPa. Green dots are used to represent the experimental data while dashed lines represent the least-square error approximation of a second-order polynomial. The membrane bulge increases with the pressure to reach a maximal deflection of 145 $\mu$m relative to the die plane at 80 kPa.

The main plot reports the maximal deflection measured at each intermediary step. Measurements are being displayed as light and dark blue dots for increasing and decreasing pressure, respectively, while plain lines are used to display the simulation results using the same color code. The dashed line is a simulation of our stack but without using the *Swift* model.

Upon pressurisation, the maximal deflection of the membrane follows a non-linear cube-root trend as expected for large deflection scenarios [29], [30]. The deflection curve follows this trend, which is perfectly modelled by both simulation models up to 50 kPa. Passed this point, both the plastic simulation and the experimental data start to diverge from the non-plastic simulation. The deflection continues to increase up to the reported maxima at 80 kPa.

When the pressure starts diminishing, both the simulated and measured maximal deflections start to decrease. The two curves follow a trend parallel to the dashed line which simulates the expected non-plastic behavior of the stack. This relaxation profile is expected and well documented in literature [49]. Once a material entered in a plastic deformation regime, when stress is released, the stress-strain curve follows a linear trend and reaches a permanently strained final state, which is the case here at 1 kPa at the end of the bulge test. The final relaxed state features a permanently strained shape with a residual deflection of 60 $\mu$m.

The final fitted values of the *Swift* model parameters are $\sigma_{\text{y,eff}} = 450$ MPa, $\varepsilon_{0,\text{eff}} = 0.0025$ and $n_{\text{eff}} = 0.05$. Those effective parameters allow to simulate the plastic behavior of our specific stack and geometry. The model also allows to estimate the residual BOX thickness at around 160 nm. This is well in line with the process based estimation of 200 nm.

### B. Strain Results

Fig. 5 depicts the simulated evolution of the strain field under increasing pressure in $R_t$. The plot only shows the main $x$, $y$ and $z$ components as the shear components are evaluated to be close to zero. As can be read on the graph, the strain field is a complex biaxial one. This is unlike what is obtained for small deflection setups where devices located on the edge of the membrane are expected to undergo uniaxial straining [11], [20]. Upon pressurisation of the membrane, both $\varepsilon_{xx}$ and $\varepsilon_{yy}$ are steadily increasing and follow a non-linear trend similar to the deflection. Again, this is unlike the linear evolution of strain with pressure reported by the literature for small deflection setups [20], [22].

The entry in the plastic regime of the stack, at around 50 kPa, is visible for both the $x$ and $y$ profiles with a decrease and increase of their respective slope. A maximum of 0.37% of deformation is obtained for $\varepsilon_{xx}$ and 0.23% for $\varepsilon_{yy}$ in $R_t$. $\varepsilon_{zz}$ showcases a steady increase up to $-0.18\%$. The plasticity of the deformation is not visible for $\varepsilon_{zz}$ since it is a linear combination of both the $x$ and $y$ components of the strain tensor following:

$$\varepsilon_{zz} = -\nu_{\text{Si}} \left(\varepsilon_{xx} + \varepsilon_{yy}\right) \tag{3}$$

where $\nu_{\text{Si}} = 0.28$ is the Poisson ratio of silicon [33].

Those results demonstrate the capacity of our flexible PI based platform to induce reasonable strain levels of up to 0.37% in silicon. This level is more than one order of magnitude bigger than what is achievable with classical bulk micro-machined or stress-compensated membranes that typically only induce up to 0.04% of strain in the device under test [11], [12]. The here reported deformation level is however one order of magnitude lower to the 3.5% of strain reached by [14]. This is explained by both their thinner 10 nm-thick silicon layer and higher 213 kPa maximal induced pressure.

Authorized licensed use limited to: Univ Catholique de Louvain/UCL. Downloaded on October 28,2025 at 09:29:17 UTC from IEEE Xplore. Restrictions apply.

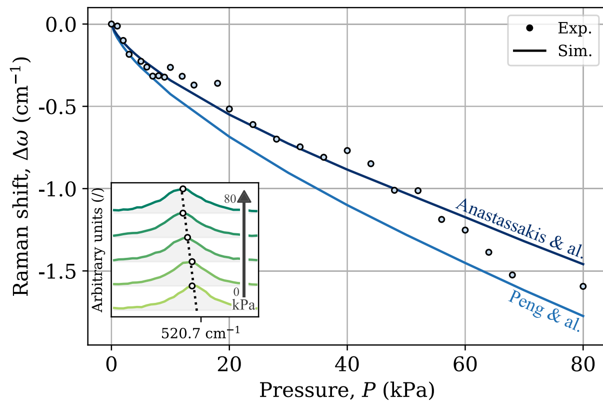


Fig. 6. Raman silicon peak shift: Raman peak shift measured into a 0.3 $\mu$m-thick c-Si resistor on a 3.6 $\mu$m-thick 2.7 mm-diameter polyimide membrane under increasing pressure levels. The inset represents the raw Raman spectrum of the silicon at pressures of 10, 20, 40, 60 and 80 kPa. The main plot shows the evolution of the position of the LO optical mode. Blue dots represent the experimentally obtained peak shifts. Plain light and dark blue lines represents the simulated peak shift obtained using the PDP coefficients from Peng and al. and Anastassakis and al. in $R_t$, respectively.

### C. Raman Validation

Fig. 6 highlights the results of the Raman validation experiment. The inset provides a selection of raw Raman spectra at increasing pressure levels of 10, 20, 40, 60 and 80 kPa. The shift of the maxima can be seen in the inset.

The main plot reports the evolution of the silicon LO peak position as a function of the pressure between 0 and 80 kPa. The experimentally obtained data is represented as blue dots. The simulation of the Raman peak shift is provided by the plain blue lines. They are computed based on the simulated strain tensor for two different sets of $p$,$q$ and $r$ PDP coefficients provided by [47] and [48].

Contrary to what is usually found in literature, the exact strain tensor has been used to retrieve the shift of the Raman peaks with the strain. A typical use of Raman spectroscopy is to either rely on an empirical peak-shift/strain relationship as in [14], [50] or on a simplification of the full Ganesan matrix as in [51]. In both cases, an indirect approximation of the strain is achieved based on a measurement of the peak-shift and a set of hypothesis made on the shape of the studied strain field. In our case, the obtained Raman results are used to check our FEM simulation. This allows the use of the full strain tensor without a-priori knowledge on its shape and components. As visible in Fig. 6, a good agreement between the simulation and the measurement is obtained. Since the experimental peak shift is an expression of the impact of the complete non-linear biaxial strain field in silicon, this gives us strong confidence in the simulated strain tensor.

The deviation between the FEM model and the experimental measurement is explained by the angle of incidence of the Raman laser. The important deflection of the membrane leads to the inclination of the c-Si devices. An angle of 3.6° is reached at 5 kPa, 5.6° at 10 kPa and 9.6° at 80 kPa, relative to the die plane. This induces a Raman response from other phonon modes such as transverse optical (TO) ones. This additional contribution to the Raman spectrum reduces the accuracy of the LO peak extraction [52], [53].

This validation, made on a canonical material like silicon, implies that our simulation framework is valid and could hence be used to predict the induction of strain in other materials without the need of a Raman measurement. This would be of particular interest for materials featuring complex, multi-peaks, Raman spectra for which empirical strain-shift relation are unknown.

Furthermore, the agreement between the simulated and experimental strain tensor demonstrates that fitting the simulation parameters on a measurement of the deflection of the membrane is sufficient to precisely estimate the strain in the electrical devices. It also demonstrates proper adhesion and hence stress transfer from the membrane to the c-Si device without slippage or delamination of the film.

## V. Conclusion

This paper reports the integration of c-Si resistors on a 3.6 $\mu$m-thick and 2.7 mm-diameter polyimide MEMS membrane using a *top-down* processing scheme. A *Comsol Multiphysics* FEM model of the membrane stack is introduced and fitted on a measurement of the membrane deflection made with a white light interferometer. This allowed to recover effective mechanical properties of the membrane as-well as the strain field induced in the silicon device.

The strain field in the c-Si resistors is found to be non-linear and biaxial. A maximal strain of 0.37% is obtained in the silicon. This represents more than a 10-fold increase compared to the strain induced by a conventional bulk micro-machined or stress compensated membrane.

Finally, the validity of the simulated strain field was checked by Raman spectroscopy. An innovative technique based on the resolution of Ganesan's secular equation using the simulated strain tensor was used. Excellent agreement of the simulation and Raman experiment allows us to have strong confidence in the simulated strain field. This agreement also demonstrates that fitting the simulation parameters on a measurement of the membrane deflection is sufficient to properly predict the strain field in the electrical device. Our work hence proposes the following methodology to perform high-strain studies on any material without the need for in-situ strain measurement: (i) Fabrication of the device to be strained via conventional processing techniques, (ii) Integration on flexible substrate, (iii) Measurement of the membrane deflection under pressure, (iv) Fitting of the simulation parameters to obtain a complete pressure-strain field relation.

AUTHORSHIP CONTRIBUTION STATEMENT

**Loïc Lahaye:** Writing - review & editing, Writing – original draft, Visualization, Validation, Methodology, Investigation, Formal Analysis, Conceptualization, Data Acquisition. **Nicolas Roisin:** Review, Validation, Methodology, Formal Analysis, Conceptualization, Data Acquisition. **Nicolas André:** Review, Methodology, Resources. **Denis Flandre:** Review, Supervision, Funding acquisition, Conceptualization. **Jean-Pierre Raskin:** Review, Supervision, Funding acquisition, Conceptualization.

Authorized licensed use limited to: Univ Catholique de Louvain/UCL. Downloaded on October 28,2025 at 09:29:17 UTC from IEEE Xplore. Restrictions apply.

## Declaration of competing interest

The authors declare that they have no known competing financial interests or personal relationships that could have appeared to influence the work reported in this paper.

## Data availability

Data will be made available on request.

## Acknowledgment

The cleanroom Winfab (Wallonia Infrastructure for Nano Fabrication) as well as the characterization lab Welcome (Wallonia Electronics & Communication Measurements) was provided by the ICTEAM department (Institute of Information and Communication Technologies, Electronics and Applied Mathematics) of the UCLouvain. Many thanks to Christian Renaux, Sébastien Faniel and Miloud Zitout, staff members of the Winfab cleanroom platform for their help and support throughout this research. A special thanks also goes to Benoît Hubert, technician in the Welcome characterization platform for his time, consideration and support.

## References

[1] P. Heremans et al., "Mechanical and electronic properties of thin-film transistors on plastic, and their integration in flexible electronic applications," *Adv. Mater.*, vol. 28, no. 22, pp. 4266–4282, 2016.

[2] V. Chan et al., "Strain for CMOS performance improvement," in *Proc. IEEE Custom Integr. Circuits Conf.*, San Jose, CA, USA 2005, pp. 662–669.

[3] O. N. Tufte, P. W. Chapman, and D. Long, "Silicon diffused-element piezoresistive diaphragms," *J. Appl. Phys.*, vol. 33, no. 11, pp. 3322–3327, Nov. 1962.

[4] J. Li, "EML webinar overview: Elastic strain engineering for unprecedented properties," *Extreme Mechan. Lett.*, vol. 54, Jul. 2022, Art. no. 101430.

[5] W. Fang and C.-Y. Lo, "On the thermal expansion coefficients of thin films," *Sensors Actuators A, Phys.*, vol. 84, no. 3, pp. 310–314, Sep. 2000.

[6] J. Laconte et al., "Thin films stress extraction using micromachined structures and wafer curvature measurements," *Microelectronic Eng.*, vol. 76, no. 1–4, pp. 219–226, Oct. 2004.

[7] U. Bhaskar et al., "On-chip tensile testing of nanoscale silicon free-standing beams," *J. Mater. Res.*, vol. 27, no. 3, pp. 571–579, Feb. 2012.

[8] T. Zabel et al., "Top-down method to introduce ultra-high elastic strain," *J. Mater. Res.*, vol. 32, no. 4, pp. 726–736, Feb. 2017.

[9] A. A. Barlian, W.-T. Park, J. R. Mallon, A. J. Rastegar, and B. L. Pruitt, "Review: Semiconductor piezoresistance for microsystems," *Proc. IEEE*, vol. 97, no. 3, pp. 513–552, Mar. 2009.

[10] T. P. Delhaye, N. André, L. A. Francis, and D. Flandre, "New universal figure of merit for embedded Si piezoresistive pressure sensors," *IEEE Sensors J.*, vol. 21, no. 1, pp. 213–221, Jan. 2021.

[11] N. Inomata, N. Van Toan, M. Toda, and T. Ono, "Evaluation of piezoresistive property of vanadium oxide thin film deposited by sputtering," *IEEE Sens. Lett.*, vol. 2, no. 1, Mar. 2018, Art. no. 2500204.

[12] J. Su et al., "Fabrication of a piezoresistive barometric pressure sensor by a silicon-on-nothing technology," *J. Sensors*, vol. 2019, no. 1, 2019, Art. no. 5408268.

[13] R. Yang et al., "Tuning optical signatures of single- and few-layer $MoS_2$ by blown-bubble bulge straining up to fracture," *Nano Lett.*, vol. 17, no. 8, pp. 4568–4575, Aug. 2017.

[14] A. K. Katiyar, K. Y. Thai, W. S. Yun, J. Lee, and J.-H. Ahn, "Breaking the absorption limit of Si toward SWIR wavelength range via strain engineering," *Sci. Adv.*, vol. 6, no. 31, Jul. 2020, Art. no. eabb0 576.

[15] H. Okaniwa, K. Nakatani, M. Yano, M. Asano, and K. Suzuki, "Preparation and properties of a-Si: H solar cells on organic polymer film substrate," *Jpn. J. Appl. Phys.*, vol. 21, no. S2, Jan. 1982, Art. no. 239.

[16] S. Gupta, W. T. Navaraj, L. Lorenzelli, and R. Dahiya, "Ultra-thin chips for high-performance flexible electronics," *npj Flexible Electron.*, vol. 2, no. 1, Mar. 2018, Art. no. 8.

[17] J. Biggs et al., "A natively flexible 32-bit Arm microprocessor," *Nature*, vol. 595, no. 7868, pp. 532–536, Jul. 2021.

[18] H. C. Ko et al., "A hemispherical electronic eye camera based on compressible silicon optoelectronics," *Nature*, vol. 454, no. 7205, pp. 748–753, Aug. 2008.

[19] Q. Guo, Z. Di, M. G. Lagally, and Y. Mei, "Strain engineering and mechanical assembly of silicon/germanium nanomembranes," *Mater. Sci. Engineering: R Reports*, vol. 128, pp. 1–31, Jun. 2018.

[20] V. Kaajakari, *Practical MEMS*. Las Vegas, NV, USA: Small gear Publishing, 2009, pp.199–206

[21] F. R. M. Rashidi, O. Hussein, and W. Z. W. Hasan, "Investigation on developing of a piezoresistive pressure sensor for foot plantar measurement system," in *Proc. IEEE Regional Symp. Micro Nanoelectronics*, Kuala Terengganu, Malaysia Aug. 2015, pp. 1–4.

[22] V. Belwanshi, "Analytical modeling to estimate the sensitivity of MEMS technology-based piezoresistive pressure sensor," *J. Comput. Electron.*, vol. 20, no. 1, pp. 668–680, Feb. 2021.

[23] V. Belwanshi and A. Topkar, "Quantitative analysis of MEMS piezoresistive pressure sensors based on wide band gap materials," *IETE J. Res.*, vol. 68, no. 1, pp. 667–677, Jan. 2022.

[24] V. Belwanshi, S. Philip, and A. Topkar, "Performance study of MEMS piezoresistive pressure sensors at elevated temperatures," *IEEE Sensors J.*, vol. 22, no. 10, pp. 9313–9320, May 2022.

[25] T. Sterken, J. Vanfleteren, T. Torfs, M. O. de Beeck, F. Bossuyt, and C. Van Hoof, "Ultra-Thin Chip Package (UTCP) and stretchable circuit technologies for wearable ECG system," in *Proc. Annu. Int. Conf. IEEE Eng. Med. Biol. Soc.* Aug. 2011, pp. 6886–6889.

[26] HDMicroSystems, "PI2545 Polyimide," 2025. Accessed: Apr. 14, 2025. [Online]. Available: https://www.hdmicrosystems.com/products/pi2545

[27] HDMicroSystems, "VM651 and VM652 Adhesion Promoters," 2022, Accessed: Apr. 14, 2025. [Online]. Available: https://www.hdmicrosystems.com/

[28] H. Xiao and L. S. Chen, "Hencky's elasticity model and linear stress-strain relations in isotropic finite hyperelasticity," *Acta Mechanica*, vol. 157, no. 1–4, pp. 51–60, Mar. 2002.

[29] W. K. Schomburg, *Introduction to Microsystem Design (Series RWTHedition)*, vol. 1. Berlin, Germany: Springer, 2011.

[30] D. Maier-Schneider, J. Maibach, and E. Obermeier, "A new analytical solution for the load-deflection of square membranes," *J. Microelectromech. Syst.*, vol. 4, no. 4, pp. 238–241, Dec. 1995.

[31] S. Franssila, *Introduction to Microfabrication*. Hoboken, NJ, USA: Wiley, 2010, ch. 5.

[32] W. A. Brantley, "Calculated elastic constants for stress problems associated with semiconductor devices," *J. Appl. Phys.*, vol. 44, no. 1, pp. 534–535, 1973. [Online]. Available: https://doi.org/10.1063/1.1661935

[33] M. A. Hopcroft, W. D. Nix, and T. W. Kenny, "What is the Young's modulus of silicon?," *J. Microelectromech. Syst.*, vol. 19, no. 2, pp. 229–238, Apr. 2010.

[34] "Structural mechanics module user's guide," Comsol, 2017. [Online]. Available: https://doc.comsol.com/5.3/doc/com.comsol.help.sme/StructuralMechanicsModuleUsersGuide.pdf

[35] S. Tu, X. Ren, J. He, and Z. Zhang, "Stress–strain curves of metallic materials and post-necking strain hardening characterization: A review," *Fatigue Fracture Eng. Mater. Structures*, vol. 43, no. 1, pp. 3–19, 2020.

[36] Micro-Measurements, "B-127: Strain gage installations wi M-Bond 200 adhesive-3," 2024, Accessed: Apr. 14, 2025. [Online]. Available: https://www.micro-measurements.com/knowledge-base/instruction-bulletins

[37] Halstrup, "Product bulletin kal100," 2024, Accessed: Sep. 23, 2024. [Online]. Available: https://www.halstrup-walcher.de/en/

[38] Polytec, "White-light interferometry," 2024, Accessed: Sep. 23, 2024. [Online]. Available: https://www.polytec.com/us/surface-metrology/technology/white-light-interferometry

[39] C. O Mahony, M. Hill, M. Brunet, R. Duane, and A. Mathewson, "Characterization of micromechanical structures using white-light interferometry," *Meas. Sci. Technol.*, vol. 14, no. 10, pp. 1807–1814, Oct. 2003.

[40] R. Loudon and N. Kurti, "Theory of the first-order raman effect in crystals," *Proc. Roy. Soc. London. Ser. A. Math. Phys. Sci.*, vol. 275, no. 1361, pp. 218–232, 1963.

[41] J. H. Parker, D. W. Feldman, and M. Ashkin, "Raman scattering by silicon and germanium," *Phys. Rev.*, vol. 155, no. 3, pp. 712–714, Mar. 1967.

Authorized licensed use limited to: Univ Catholique de Louvain/UCL. Downloaded on October 28,2025 at 09:29:17 UTC from IEEE Xplore. Restrictions apply.

[42] N. Roisin, M.-S. Colla, J.-P. Raskin, and D. Flandre, “Raman strain–shift measurements and prediction from first-principles in highly strained silicon,” *J. Mater. Sci., Mater. Electron.*, vol. 34, no. 5, Feb. 2023, Art. no. 373.
[43] H. S. Virk, P. S. Chandi, and A.K. Srivastava, “Physical and chemical response of 70 MeV carbon ion irradiated kapton-h polymer,” *Bull. Mater. Sci.*, vol. 24, no. 5, pp. 529–534, Oct. 2001.
[44] I. Savatinova, S. Tonchev, R. Todorov, E. Venkova, E. Liarokapis, and E. Anastassakis, “Polyimide thin-film waveguides: Optical and Raman spectroscopic studies,” *J. Appl. Phys.*, vol. 67, no. 4, pp. 2051–2055, Feb. 1990.
[45] I. D. Wolf, “Micro-Raman spectroscopy to study local mechanical stress in silicon integrated circuits,” *Semicond. Sci. Technol.*, vol. 11, no. 2, pp. 139–154, Feb. 1996.
[46] S. Ganesan, A. Maradudin, and J. Oitmaa, “A lattice theory of morphic effects in crystals of the diamond structure,” *Ann. Phys.*, vol. 56, no. 2, pp. 556–594, Feb. 1970.
[47] E. Anastassakis, A. Pinczuk, E. Burstein, F. H. Pollak, and M. Cardona, “Effect of static uniaxial stress on the Raman spectrum of silicon,” *Solid State Commun.*, vol. 8, no. 2.
[48] C.-Y. Peng et al., “Comprehensive study of the Raman shifts of strained silicon and germanium,” *J. Appl. Phys.*, vol. 105, no. 8, 2009, Art. no. 083537.
[49] J. Lubliner, *Plasticity Theory (Dover Books on Engineering)*, New York, NY, USA: Dover Publications, 2008, pp. 80–85
[50] Y.-Y. Fang et al., “Perfectly tetragonal, tensile-strained Ge on Ge1-ySny buffered Si(100),” *Appl. Phys. Lett.*, vol. 90, no. 6, Feb. 2007, Art. no. 0 61915.
[51] A. Shchepetov et al., “Ultra-thin free-standing single crystalline silicon membranes with strain control,” *Appl. Phys. Lett.*, vol. 102, no. 19, May 2013, Art. no. 192108.
[52] W. S. Yoo, H. Harima, and M. Yoshimoto, “Polarized raman signals from Si wafers: Dependence of in-plane incident orientation of probing light,” *ECS J. Solid State Sci. Technol.*, vol. 4, no. 9, pp. P356–P363, 2015.
[53] U. Ramabadran and B. Roughani, “Intensity analysis of polarized raman spectra for off axis single crystal silicon,” *Mater. Sci. Eng., B*, vol. 230, pp. 31–42, Apr. 2018.

**Loïc Lahaye** received the M.S. degree in electromechanical engineering from the UCLouvain, Louvain-la-Neuve, Belgium, in 2022, where he is currently working toward the Ph.D. degree with the Institute of Information and Communication Technologies, Electronics and Applied Mathematics (ICTEAM). His research interests include oriented towards strain engineering studies in silicon and vanadium dioxide, and in the development of flexible MEMS devices.

**Nicolas Roisin** received the M.S. degree in electrical engineering from the UCLouvain, Louvain-la-Neuve, Belgium, in 2019, where he is currently working toward the Ph.D. degree with the Institute of Information and Communication Technologies, Electronics and Applied Mathematics (ICTEAM). His research interests include strained silicon in sensing and optical applications.

**Nicolas André** received the M.S. degree in electrical engineering from the Louvain School of Engineering, UCLouvain, Louvain-la-Neuve, Belgium, in 2004, and the Ph.D. degree in applied sciences in the field of microelectromechanical systems (MEMS) co-integration from UCL, London, U.K., in 2011. From 2011 to 2012, he was with UdeS, Sherbrooke, QC, Canada, as a Postdoctoral Researcher on bio-inspired methods to improve the LED efficiency. He has coauthored more than 100 research articles in international journals and holds two patents. His expertise is about microfabrication and sensors (flow, humidity, pressure and light) integrated with SOI CMOS Circuits. He was a team member in several Walloon, FEDER, and EU projects as STARFLO+, FEDER, MINATIS, and MICRO+.

**Denis Flandre** (Senior Member, IEEE) received the M.S. degree in electrical engineering, and the Ph.D. and Research Habilitation degrees from the UCLouvain, Louvain-la-Neuve, Belgium, in 1986, 1990, and 1999, respectively. His doctoral research was on the modeling of Silicon-on-Insulator (SOI) MOS devices for characterization and circuit simulation, his postdoctoral thesis on a systematic and automated synthesis methodology for MOS analog circuits. Since 2001, he has been a Full Time Professor with UCL. He has participated or coordinated numerous research projects funded by regional and European institutions. He has organized or lectured many short courses on SOI technology, devices and circuits in universities, industrial companies, and conferences. He has authored or coauthored more than 1200 technical papers or conference contributions. He is a Co-Inventor of more than 10 patents. He is involved in the research and development of SOI MOS devices, digital and analog circuits, and sensors and MEMS, for special applications, more specifically high speed, low-voltage low power, microwave, biomedical, radiation-hardened, high temperature electronics and microsystems.

**Jean-Pierre Raskin** (Fellow, IEEE) received the M.S. and Ph.D. degrees in applied sciences from the UCLouvain, Louvain-la-Neuve, Belgium, in 1994 and 1997, respectively. In 1998, he joined the EECS Department, The University of Michigan, Ann Arbor, MI, USA. In 2000, he joined Microwave Laboratory, UCLouvain, as an Associate Professor, and he has been a Full Professor since 2007. From 2009 to 2010, he was a Visiting Professor with Newcastle University, Newcastle Upon Tyne, U.K. He was the Head of the Electrical Engineering Department, UCLouvain between 2014 and 2017. He has authored or coauthored more than 400 scientific journal articles. His research interests include modeling, wideband characterization, fabrication of advanced SOI MOSFETs, micro and nanofabrication of MEMS/NEMS sensors and actuators, including the extraction of intrinsic material properties at nanometer scale. After receiving numerous prizes, he has been elected member of the Royal Academy of Belgium in 2023.

Authorized licensed use limited to: Univ Catholique de Louvain/UCL. Downloaded on October 28,2025 at 09:29:17 UTC from IEEE Xplore. Restrictions apply.